Site-selective yellow to violet and near-infrared to green upconversion in $BaLu_2F_8:Nd^{3+}$

Oliver S. Wenger, Daniel R. Gamelin, and Hans U. Güdel
Departement für Chemie und Biochemie, Universität Bern, Freiestrasse 3, 3000 Bern 9, Switzerland

Andrei V. Butashin and Alexander A. Kaminskii
Institute of Crystallography, Russian Academy of Sciences, Leninskii Prospekt 59, 117333 Moscow, Russia
(Received 9 November 1999)

Single crystals of $BaLu_2F_8$ doped with 0.6% Nd^{3+} were studied by high-resolution optical absorption, luminescence, and excitation spectroscopy in the 15–300 K temperature range. The two crystallographically distinct sites for the dopant ions present in this host are identified spectroscopically. Blue and violet upconversion luminescence was observed under pulsed excitation into the $^4G_{5/2}$ and $^2G_{7/2}$ multiplets in the yellow spectral range at all temperatures between 15 and 300 K. Green upconversion luminescence was obtained at 15 K after cw excitation into the $^4F_{5/2}$ and $^2H_{9/2}$ excited states around 800 nm. By means of time-resolved spectroscopy an excited-state absorption originating from the long-lived $^4F_{3/2}$ excited state was found to be responsible for yellow to violet upconversion. Near-infrared to green upconversion occurs via energy transfer involving two nearby excited Nd^{3+} ions doped into crystallographic sites of the same type. At 15 K both upconversion processes are site-selective, i.e., upconversion luminescence is observed exclusively from the initially excited site, and intersite energy transfer is only important above 30 K. The different photophysical properties of $BaLu_2F_8$:0.6% Nd^{3+} and $BaLu_2F_8$:1% Er^{3+} with respect to the two crystallographically distinct rare-earth-dopant sites are discussed.

I. INTRODUCTION

Since the first report of upconversion more than 25 years ago, this approach of generating short-wavelength emission using excitation light of lower energy has received a great deal of attention.[1–3] The development of uv and visible compact solid-state lasers, especially those that can be pumped by inexpensive laser diodes, is interesting for applications in the fields of data storage and display.[4,5] Upconversion is a very common phenomenon among lanthanide-doped insulating materials, including glasses as well as crystalline materials.[6] In fluorides the number of excited states available for upconversion and luminescence processes is higher than that in oxides, due to more efficient multiphonon relaxation in the latter. This nonradiative deactivation process is suppressed even further in low-phonon hosts, such as $LaCl_3$ or $Cs_3Lu_2Br_9$.[7,8] However, when compared to those materials, fluorides have the big advantage of being hard, stable in air, and essentially insensitive to moisture. From a materials point of view, they are therefore ideally suited for laser applications.[9] The title material has been known for several years. Nevertheless, it has only recently become available in the form of single crystals with an optical quality sufficient for laser purposes.[10] Recently, the suitability of this material for laser applications has been demonstrated by room-temperature downconversion laser action of the $^4F_{3/2} \rightarrow {}^4I_{11/2}$ transition around 1.0483 μm.[10]

$BaLu_2F_8$ shows the typical properties of fluoride lattices mentioned above. Two different modifications of this material are known: the monoclinic β-$BaLu_2F_8$ phase and the orthorhombic α structure, which is the subject of this study. This orthorhombic structure (space group *Pnma*) is metastable at room temperature. It is a framework formed by LuF_8 polyhedra linked together by sharing corners and edges.[10,11] In contrast with established fluoride laser materials such as $LiYF_4:Nd^{3+}$ or $LaF_3:Nd^{3+}$, however, Nd^{3+} ions doped into this lattice may occupy one of two crystallographically inequivalent Lu^{3+} sites, referred to here as sites *A* and *B*.[12–14] The structures of these two sites, in which the Lu^{3+} ions are coordinated by eight F^- with C_1 symmetry, are depicted in Fig. 1. The primary structural difference is given by the Lu^{3+}-F^- distances: in site *A* these distances vary from 2.18 up to 2.28 Å, whereas in site *B* there are seven Lu^{3+}-F^- distances in the range from 2.16 to 2.26 Å and an eighth with 2.58 Å being significantly longer.[10] Thus, site *A* approaches more closely the limit of a spherical Lu^{3+} coordination than site *B*.

In this paper we report on the yellow to violet and near-infrared to green upconversion processes in α-$BaLu_2F_8:Nd^{3+}$, and we compare these results with those found for the established yellow to violet upconversion laser materials $LiYF_4:Nd^{3+}$ and $LaF_3:Nd^{3+}$.[13,14] In the observed upconversion processes, particular attention has been given to the role of the two different rare-earth-dopant sites. The spectroscopic data presented in this study provide a basis for

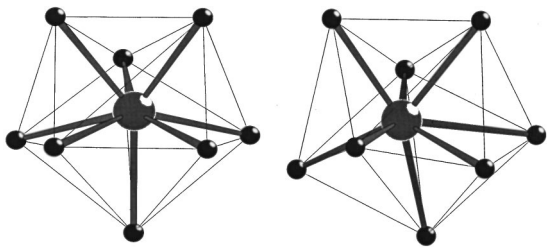

FIG. 1. The two crystallographically distinct LuF_8 polyhedra in the $BaLu_2F_8:Nd^{3+}$ host lattice.

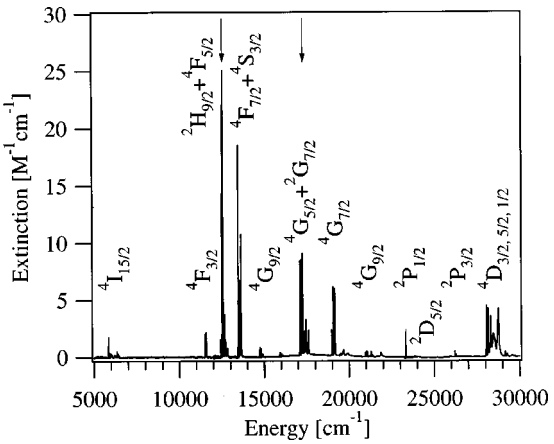

FIG. 2. Unpolarized survey absorption spectrum of a $BaLu_2F_8$:0.6% Nd^{3+} crystal at 15 K. Selected excited states are labeled, and the multiplets used for upconversion excitation are marked by an arrow.

the implementation of the $BaLu_2F_8$:Nd^{3+} material in upconversion laser experiments.

II. EXPERIMENT

A. Crystal growth

Sample preparation is described in detail elsewhere.[10] Briefly, crystals of α-$BaLu_2F_8$ doped with 0.6% Nd^{3+} were grown using the Bridgman-Stockbarger technique in an HF atmosphere, using BaF_2, LuF_3, and NdF_3 as starting materials. Crystals of good optical quality were obtained up to 6 mm in diameter and 30 mm in length.

B. Optical spectroscopy

All spectra were measured unpolarized with a random crystal orientation. Sample cooling was achieved by a closed-cycle cryostat (Air Products Displex) for absorption measurements and with a He-gas flow technique for the emission experiments. A Cary 5e (Varian) spectrometer was used for the absorption measurements. Continuous-wave near-infrared excitation was performed using a Ti:sapphire laser (Spectra Physics 3900S) pumped by an argon laser (Spectra Physics 2045) in all-lines mode. An inchworm driven (Burleigh PZ 501) birefringent filter was used for the wavelength control. The detection system consisted of a 0.85-m double monochromator (Spex 1402) with 500-nm blazed 1200-grooves/mm gratings, a cooled photomultiplier (RCA 31034 or Hamamatsu C2761), and a photon-counting system (Stanford Research SR400). Rectangular excitation pulses were generated by passing the laser beam through an acousto-optic modulator (Coherent 305) connected to a function generator (Stanford Research DS 345). For the lifetime measurements a multichannel scaler (Stanford Research SR430) was used.

Pulsed excitation in the yellow spectral range was performed using the output of a frequency-doubled Nd^{3+}:YAG laser (Quanta Ray, DCR-3, 20 Hz) pumped dye laser (Lambda Physik FL 3002, Rhodamine 6G in methanol). For direct $^4F_{3/2}$ excitation around 11 500 cm^{-1} the same setup was used with the DCM dye and a Raman shifter (Quanta Ray RS-1, H_2 340 psi) after the dye laser. For direct $^4D_{3/2,5/2,1/2}$ excitation around 28 195 cm^{-1} the frequency-tripled output of the Nd^{3+}:YAG (YAG denotes yttrium aluminum garnet) laser was used directly. The sample luminescence was dispersed by a 0.75-m single monochromator (Spex 1702) using 300/750 nm blazed 1200/600 grooves/mm gratings and detected as described above.

Luminescence spectra were corrected for the sensitivity of the detection system, and excitation spectra were corrected for the excitation laser power. Both types of spectra are displayed as photon counts versus energy (cm^{-1}).

TABLE I. Selected energy levels in $BaLu_2F_8$:Nd^{3+} extracted from high-resolution absorption, luminescence, and excitation spectra. Energies are given in wave numbers (cm^{-1}) relative to the lowest-energy Stark level. *A* and *B* correspond to the two crystallographically distinct rare-earth sites; see Fig. 1.

		A	*B*			*A*	*B*
$^4I_{9/2}$	(1)	0	0		(2)	11 556	11 568
	(2)	90	31				
	(3)	214	180	$^4F_{5/2}$	(1)	12 513	12 500
	(4)	294	283		(2)	12 532	12 530
	(5)	415	490		(3)	12 565	12 569
$^4I_{11/2}$	(1)	1 987	1 965	$^2H_{9/2}$	(1)	12 619	12 622
	(2)	2 010	1 997		(2)	12 653	12 660
	(3)	2 048	2 021		(3)	12 716	12 688
	(4)	2 101	2 093		(4)	12 749	12 772
	(5)	2 166	2 197		(5)	12 792	12 829
	(6)	2 208	2 243				
				$^4G_{5/2}$	(1)	17 122	17 113
$^4I_{13/2}$	(1)	3 932	3 914		(2)	17 192	17 178
	(2)	3 963	3 933		(3)	17 260	17 258
	(3)	3 992	3 971				
	(4)	4 076	4 041	$^2G_{7/2}$	(1)	17 343	17 356
	(5)	4 105	4 140		(2)	17 389	17 414
	(6)	4 180	4 225		(3)	17 421	17 459
	(7)	4 205	4 244		(4)	17 566	17 607
$^4I_{15/2}$	(1)	5 855	5 817	$^4G_{7/2}$	(1)	18 996	18 968
	(2)	5 879	5 849		(2)		
	(3)	6 010	5 966		(3)		
	(4)	6 071	6 033		(4)		
	(5)	6 196	6 195				
	(6)	6 264	6 345	$^2P_{3/2}$	(1)	26 210	26 216
	(7)	6 330	6 395		(2)		
	(8)	6 391	6 449				
				$^4D_{3/2}$	(1)	28 054	28 062
$^4F_{3/2}$	(1)	11 508	11 506		(2)		

III. RESULTS

Figure 2 shows the unpolarized absorption spectrum of $BaLu_2F_8$:0.6% Nd^{3+} in the infrared and visible spectral range at 15 K. The sharp and relatively weak *f-f* transitions are assigned according to the literature.[15] The arrows mark the $^4F_{5/2}$+$^2H_{9/2}$ and the $^4G_{5/2}$+$^2G_{7/2}$ multiplets that were excited for the near-infrared to green and the yellow to violet upconversion studies, respectively. The Stark level energies

of some relevant multiplets are given in Table I.

In Table II the lifetimes of some relevant excited states of $BaLu_2F_8$:0.6% Nd^{3+} extracted from time-dependent luminescence experiments are collected. At 15 K different lifetimes were measured for the two crystallographically distinct sites *A* and *B*, respectively. At room temperature the lifetimes of the various excited states are independent of the exact excitation and detection energy, respectively, i.e., only a single lifetime value was obtained for each excited state.

Figure 3 presents the 15-K unpolarized survey upconversion luminescence spectrum of $BaLu_2F_8$:0.6% Nd^{3+} in the visible spectral region obtained after excitation at 17 459 cm^{-1} (site *B*) into the $^2G_{7/2}$ multiplet (arrow in Fig. 2). Note that the intensities of the transitions around 20 000 and 22 000 cm^{-1} are multiplied by factors of 50 and 5, respectively. After excitation into the $^4D_{3/2,5/2,1/2}$ multiplets around 28 195 cm^{-1} the same luminescence transitions and intensity ratios are observed. The branching ratios between the various luminescence transitions from a given state differ by less than 10% between the two different sites. The five features are labeled (1)–(5) and are assigned as described in Fig. 4. Features (2), (3), and (4) at approximately 22 000, 24 000, and 26 000 cm^{-1} are comprised of energetically overlapping luminescence transitions originating from the $^4D_{3/2}$ and $^2P_{3/2}$ excited states, as schematically depicted in Fig. 4.

Figure 5 shows the temporal behavior of the *A*-site $^4D_{3/2}$ (left) and $^2P_{3/2}$, (right) populations, respectively, at 15 K after an excitation pulse of 8 ns width. The excitation energy was 17 389 cm^{-1}, and detection occurred at 27 964 cm^{-1} ($^4D_{3/2}\rightarrow{}^4I_{9/2}$ transition) and 24 162 cm^{-1} ($^2P_{3/2}\rightarrow{}^4I_{11/2}$ transition), respectively.

In Fig. 6 we report the time-resolved $^4D_{3/2}\rightarrow{}^4I_{13/2}$ and $^2P_{3/2}\rightarrow{}^4I_{11/2}$ upconversion luminescence following excitation into sites *A* (upper half) and *B* (lower half) at 15 K. Collected immediately after the exciting laser pulse, spectra (a1) and (b1) show simultaneous $^4D_{3/2}\rightarrow{}^4I_{13/2}$ and $^2P_{3/2}\rightarrow{}^4I_{11/2}$ luminescence for the *A* and *B* sites. These spectra evolve with time during the first several microseconds after the laser pulse. Spectra (a2) and (b2), recorded with a delay of 15 μs after the laser pulse, show exclusively the $^2P_{3/2}\rightarrow{}^4I_{11/2}$ transitions of the respective sites. The $^4I_{13/2}$ and $^4I_{11/2}$ Stark-level splittings are represented by the brackets.

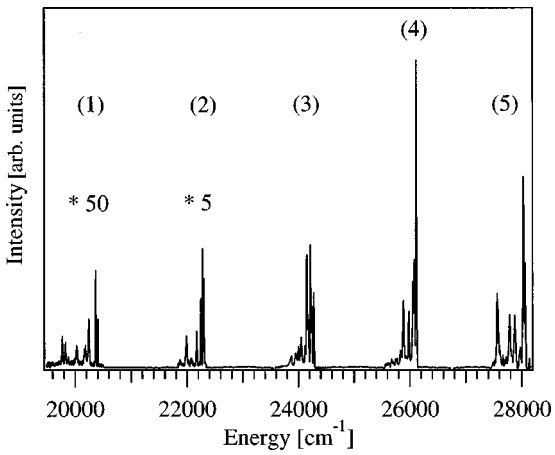

FIG. 3. 15-K survey upconversion luminescence spectrum of $BaLu_2F_8$:0.6% Nd^{3+} obtained after excitation of $^2G_{7/2}$ at 17 459 cm^{-1} (site *B*). The intensities of the transitions around 20 000 and 22 000 cm^{-1} are multiplied by factors of 50 and 5, respectively. The numbers in parentheses correspond to the transitions schematically depicted in Fig. 4.

Figure 7 shows the unpolarized absorption spectrum of $BaLu_2F_8$:Nd^{3+} in the $^4G_{5/2}$, $^2G_{7/2}$ spectral region at 15 K (upper trace) together with excitation spectra of the same sample monitoring the 15-K $^4D_{3/2}\rightarrow{}^4I_{9/2}$ upconversion luminescence at 27 964 cm^{-1} (site *A*, middle trace) and at 28 027 cm^{-1} (site *B*, lower trace), respectively. The brackets represent the Stark-level splittings of the $^4G_{5/2}$ and $^2G_{7/2}$ multiplets for the two different dopant sites.

In the upper part of Fig. 8 the 15-K absorption spectrum of $BaLu_2F_8$:Nd^{3+} in the $^4G_{7/2}$ region is presented. The middle and the lower part show 15-K upconversion luminescence spectra obtained after excitation into the $^4F_{5/2}$ multiplet at 12 513 cm^{-1} (site *A*) and 12 500 cm^{-1} (site *B*), respectively, as indicated by the asterisks in Fig. 9.

The upper trace of Fig. 9 is the 15-K $^4I_{9/2}\rightarrow{}^4F_{5/2}+{}^2H_{9/2}$ absorption spectrum of $BaLu_2F_8$:Nd^{3+}. The middle and the lower trace are 15-K excitation spectra of the same crystal with detection of $^4G_{7/2}\rightarrow{}^4I_{9/2}$ upconversion luminescence at 18 907 cm^{-1} (site *A*) and 18 937 cm^{-1} (site *B*) as indicated by the asterisks in Fig. 8.

TABLE II. Lifetimes τ at cryogenic and ambient temperatures of some relevant excited states in $LiYF_4$:Nd^{3+}, BaY_2F_8:0.4% Nd^{3+}, and $BaLu_2F_8$:0.6% Nd^{3+}. The $^4D_{3/2}$ and $^2P_{3/2}$ lifetimes of $BaLu_2F_8$:0.6% Nd^{3+} are both the same after direct $^4D_{3/2}$ excitation and after excitation of the $^4G_{5/2}+{}^2G_{7/2}$ excited states.

	$LiYF_4$:Nd^{3+} τ (μs)		BaY_2F_8:0.4% Nd^{3+} τ (μs)		$BaLu_2F_8$:0.6% Nd^{3+} τ (μs)		
	$T=10$ K	$T=300$ K	$T=6$ K	$T=300$ K	$T=15$ K		$T=300$ K
Multiplet					Site *A*	Site *B*	
$^4F_{3/2}$	440[a]		530[c]	470[c]	403	501	400
$^2P_{3/2}$	50[b]	35[b]	116[c]	50[c]	100	68	35
$^4D_{3/2}$	1.3[b]	1.3[b]	4.2[c]	2.7[c]	4.0	3.5	2.3

[a]Dopant concentration 1.7%, from Ref. 14.
[b]Dopant concentration 0.1%, from Ref. 19.
[c]From Ref. 18.

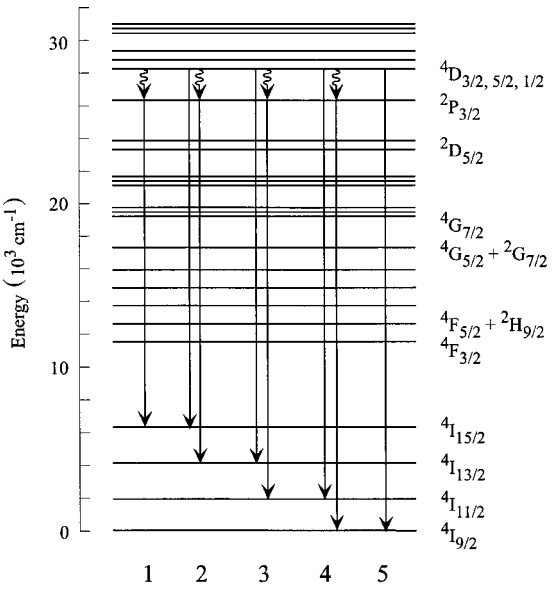

FIG. 4. Energy-level diagram of Nd^{3+} including the main upconversion luminescence transitions observed after excitation of the $^4G_{5/2}$ and $^2G_{7/2}$ excited states. The multiplets 2, 3, and 4 each contain two transitions of very similar energy.

IV. ANALYSIS AND DISCUSSION

A. Energy levels and excited-state lifetimes

The survey absorption spectrum (Fig. 2) reveals a large energy gap of more than 5000 cm^{-1} between $^4F_{3/2}$ and its energetically next lower lying $^4I_{15/2}$ multiplet. Using a value of 420 cm^{-1} for the maximum phonon energy in the $BaLu_2F_8$ host, a reduced energy gap of $p=12$ phonons is calculated.[10] For *f-f* transitions in lanthanides, multiphonon relaxation is typically only important for $p \leqslant 6$, and such nonradiative processes can be neglected for the $^4F_{3/2}$-$^4I_{15/2}$ gap in our case.[16,17] Additionally, nonradiative cross-relaxation of the $^4F_{3/2}$ excited state is energetically not possible at 15 K. Therefore the low-temperature $^4F_{3/2}$ lifetimes given in Table II are purely radiative. In $BaLu_2F_8$:0.6% Nd^{3+} the excitation energy is stored in the $^4F_{3/2}$ excited state as efficiently as in $LiYF_4$:1.7% Nd^{3+} and BaY_2F_8:0.4% Nd^{3+}, as shown by the similar $^4F_{3/2}$ lifetimes in these three materials (Table II).[14,18] A long $^4F_{3/2}$ lifetime is favorable for upconversion processes involving $^4F_{3/2}$ as an intermediate state.

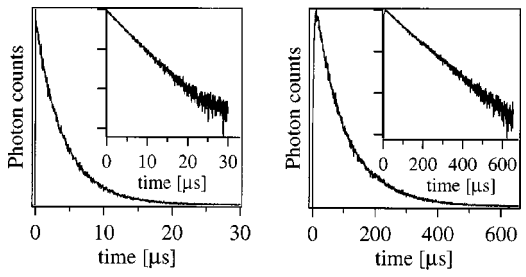

FIG. 5. Site-A $^4D_{3/2} \rightarrow {}^4I_{9/2}$ (left) and $^2P_{3/2} \rightarrow {}^4I_{11/2}$ (right) upconversion luminescence transients after $^2G_{7/2}$ excitation (17 389 cm^{-1}, site *A*) of $BaLu_2F_8$:0.6%Nd^{3+} at 15 K. The excitation pulse has a width of 8 ns and occurs at $t=0$. The insets show the same data in a semilogarithmic representation.

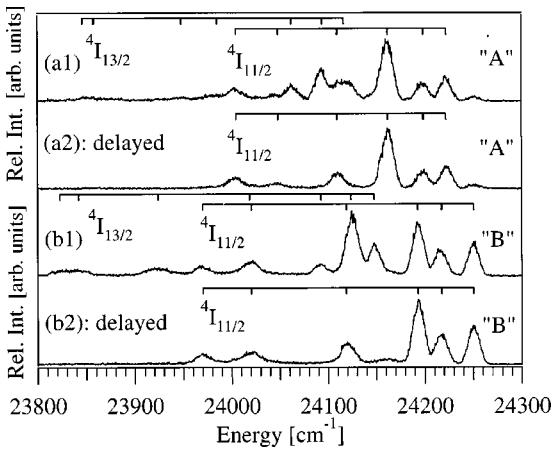

FIG. 6. 15-K high-resolution upconversion luminescence spectra of $BaLu_2F_8$:0.6%Nd^{3+} in the spectral region of the $^4D_{3/2} \rightarrow {}^4I_{13/2}$ and $^2P_{3/2} \rightarrow {}^4I_{11/2}$ transitions: (a1) immediately after excitation at 17 389 cm^{-1} (site *A*), (a2) 15 μs after the 17 389 cm^{-1} excitation pulse, (b1) immediately after excitation at 17 459 cm^{-1} (site *B*), (b2) 15 μs after the 17 459 cm^{-1} excitation pulse. (a1) and (b1) show a superposition of the $^4D_{3/2} \rightarrow {}^4I_{13/2}$ and $^2P_{3/2} \rightarrow {}^4I_{11/2}$ transitions. (a2) and (b2) show only the $^2P_{3/2} \rightarrow {}^4I_{11/2}$ transitions. The brackets indicate the Stark splittings of the $^4I_{13/2}$ and $^4I_{11/2}$ multiplets for sites *A* and *B*, respectively.

Still referring to the survey absorption spectrum (Fig. 2) we note that the multiplets above $^4F_{3/2}$ up to $^2D_{5/2}$ are energetically very close to each other with reduced energy gaps of at most 3.4 phonons. This makes multiphonon relaxation the most efficient relaxation process among these excited states. The situation is again different for the $^4D_{3/2}$ and $^2P_{3/2}$ excited states since the reduced energy gaps to their energetically next lower lying multiplets are $p=4.75$ and $p=5.5$, respectively. In these two excited states radiative emission and multiphonon relaxation are competing deactivation processes, even at cryogenic temperatures. At elevated temperatures, nonradiative processes become relatively more important. This is shown by the reduction of the $^4D_{3/2}$ and $^2P_{3/2}$

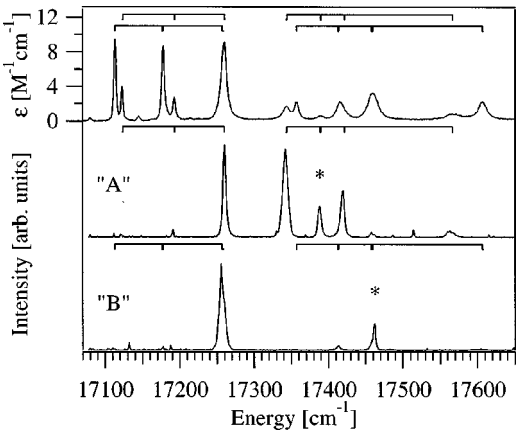

FIG. 7. Upper trace: $^4I_{9/2} \rightarrow {}^4G_{5/2}$, $^2G_{7/2}$ absorption spectrum of $BaLu_2F_8$:0.6%Nd^{3+} at 15 K. Middle and lower trace: 15-K upconversion excitation spectra of the same sample with detection of luminescence at 27 964 cm^{-1} (site *A*) and 28 027 cm^{-1} (site *B*), respectively. Asterisks indicate peaks used to excite the spectra in Fig. 6. The brackets indicate the Stark splittings of the $^4G_{5/2}$ and $^2G_{7/2}$ multiplets for sites *A* and *B*, respectively.

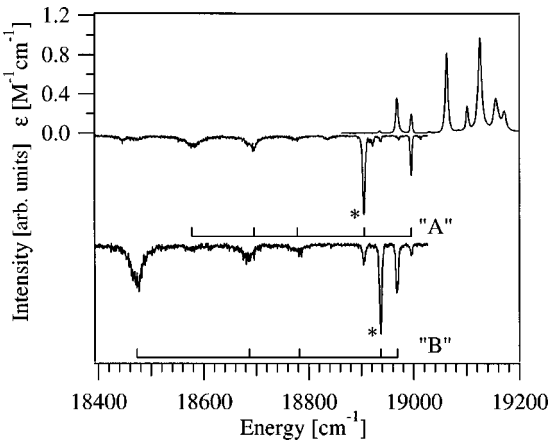

FIG. 8. $^4I_{9/2}\rightarrow{}^4G_{7/2}$ absorption spectrum of $BaLu_2F_8$:0.6%Nd^{3+} at 15 K (top). High-resolution $^4G_{7/2}\rightarrow{}^4I_{9/2}$ upconversion luminescence spectra of the same crystal at 15 K excited at 12 513 cm^{-1} (middle) and at 12 500 cm^{-1} (bottom) into $^4I_{9/2}\rightarrow{}^4F_{5/2}$ ground-state absorption bands of site *A* and site *B*, respectively. The brackets indicate the Stark splittings of the $^4I_{9/2}$ ground state for the *A* and *B* sites, respectively. The asterisks indicate the emission features used to collect the data presented in Fig. 9.

lifetimes by factors of approximately 3 and 2, respectively, in the 15–300 K temperature range (Table II). In addition to faster multiphonon relaxation at elevated temperatures, the thermally activated cross relaxations $^4D_{3/2}+{}^4I_{9/2}\rightarrow{}^2P_{3/2}+{}^4I_{11/2}$ and $^2P_{3/2}+{}^4I_{9/2}\rightarrow{}^4S_{3/2}/{}^4F_{7/2}+{}^2H_{9/2}/{}^4F_{5/2}$ gain importance and cause a more efficient nonradiative depopulation of the $^4D_{3/2}$ and $^2P_{3/2}$ excited states.

At 15 K, $^4D_{3/2,5/2,1/2}$ excitation with laser pulses of 8 ns width is followed by an instantaneous single-exponential decay, as shown in Fig. 5, left. Transients of $^2P_{3/2}$ emission, on the other hand, always exhibit a rise time corresponding to the $^4D_{3/2}$ lifetime preceding the decay (Fig. 5, right). This is a manifestation of the fact that the $^2P_{3/2}$ population is built up via (nonradiative) relaxation from the $^4D_{3/2}$ excited state.

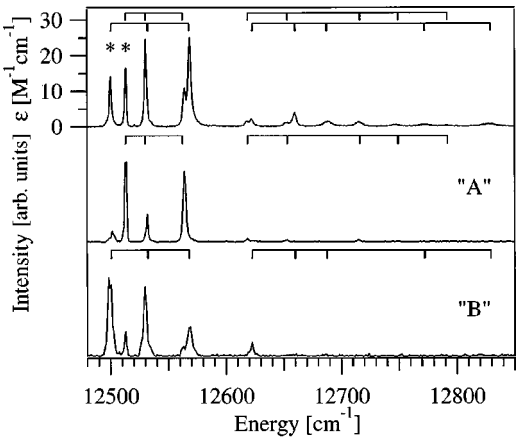

FIG. 9. The upper trace shows the $^4I_{9/2}\rightarrow{}^4F_{5/2}+{}^2H_{9/2}$ absorption spectrum of $BaLu_2F_8$:0.6%Nd^{3+} at 15 K. The middle and the lower trace are 15 K excitation spectra detecting $^4G_{7/2}\rightarrow{}^4I_{9/2}$ upconversion luminescence at 18 907 cm^{-1} (site *A*) and 18 937 cm^{-1} (site *B*), respectively, as indicated by the asterisks in Fig. 8. The brackets represent the Stark splittings of the $^4F_{5/2}$ and $^2H_{9/2}$ multiplets of the two crystallographically different sites.

As shown in Table II, the $^4D_{3/2}$ and $^2P_{3/2}$ lifetimes of $BaLu_2F_8$:0.6% Nd^{3+} are similar to those of BaY_2F_8:0.4% Nd^{3+} and, in particular at cryogenic temperatures, longer than those of $LiYF_4$:0.1% Nd^{3+}.[18,19] This is favorable for yellow to violet upconversion laser purposes since it helps to establish a population inversion between one of these excited states and a potential lower lying, terminating laser level.

At 15 K, the lifetimes of the various excited states differ by 10–30 % between Nd^{3+} ions doped into the crystallographically distinct sites *A* and *B*. The site-*B* $^4F_{3/2}$ lifetime is 25% longer than the corresponding site-*A* lifetime, although in the observed ground-state absorption spectra the site-*B* peaks generally have higher oscillator strengths than site-*A* peaks. As shown above, the $^4F_{3/2}$ lifetime is purely radiative, and one could therefore, based on the ground-state absorption data, expect it to be shorter for site *B* than for site *A*. However, the $^4F_{3/2}$ lifetime is mainly determined by the $^4F_{3/2}\rightarrow{}^4I_{11/2}$ transition rate since this is the strongest emission from the $^4F_{3/2}$ excited state. We therefore conclude that the $^4I_{11/2}\rightarrow{}^4F_{3/2}$ excited-state absorption is weaker for site *B* than for site *A*.

The $^2P_{3/2}$ and $^4D_{3/2}$ lifetimes of site *B* are both shorter than those of site *A*. Since these lifetimes are not purely radiative, this is, to a certain extent, not only due to a higher radiative emission rate of site *B* compared to site *A*, but also to a more efficient multiphonon relaxation among site-*B* Nd^{3+} ions. Table I shows that the overall crystal-field splittings of the various multiplets are always larger (up to 75 cm^{-1}) for site *B* than those for site *A*, although the baricenter energies are similar. As a consequence, the energy gaps between the various excited states of site *B* are smaller, which in turn facilitates multiphonon relaxation for Nd^{3+} ions doped into this site.

On the basis of the larger site-*B* crystal-field splittings and the higher oscillator strengths in site-*B* ground-state absorption spectra, we assign site *B* to the more distorted NdF_8 polyhedron (Fig. 1) since this is expected to have a higher odd-parity crystal-field component than the NdF_8 polyhedron with the eight similar Nd-F distances, which is closer to the limit of a spherical coordination of the Nd^{3+} ion.

B. Yellow to violet upconversion

Excitation into the $^4G_{5/2}$ and $^2G_{7/2}$ multiplets around 17 300 cm^{-1} as well as excitation into the $^4D_{3/2,5/2,1/2}$ excited states around 28 200 cm^{-1} leads to the same luminescence transitions originating from $^4D_{3/2}$ and $^2P_{3/2}$, respectively; see Fig. 3. In total, eight luminescence transitions are observed in the 20 000–28 200-cm^{-1} spectral range. The intensity ratios between the various transitions do not depend on whether excitation takes place in the yellow or violet spectral region. However, at cryogenic temperatures, the luminescence spectrum strongly depends on which site is excited. At these temperatures, luminescence is only observed from the initially excited site and there is no energy transfer among Nd^{3+} ions doped into different sites. This is also the case after excitation in the yellow region. Thus the whole yellow to violet upconversion process is site-selective at 15 K. Temperature-dependent luminescence spectra (data not shown) indicate that at temperatures above 30 K intersite energy-transfer processes become important. At 300 K the

luminescence spectra are independent of the exact excitation energy, as one would expect in case of an efficient energy transfer among Nd^{3+} ions in sites *A* and *B*.

As reported in Sec. III, there is a superposition of $^4D_{3/2} \rightarrow {}^4I_{J+1}$ and $^2P_{3/2} \rightarrow {}^4I_J$ $(J=13/2,11/2,9/2)$ luminescence transitions at energies of approximately 22 000, 24 000, and 26 000 cm^{-1}, respectively. Using a gated photon-counting technique it is possible to deconvolute the luminescence transitions originating from $^4D_{3/2}$ and $^2P_{3/2}$ due to the different population dynamics of these excited states. Immediately after the exciting laser pulse $(t=0)$, $^4D_{3/2}$ is populated maximally and starts to decay instantaneously. At $t=15\,\mu s$ the $^4D_{3/2}$ population has decayed to 2.4% (site *A*) and 1.4% (site *B*), respectively, of the population at $t=0$ (Fig. 5, left). The $^2P_{3/2}$ population, on the other hand, is negligible at $t=0$. Since $^2P_{3/2}$ is fed via (nonradiative) relaxation from $^4D_{3/2}$ (Sec. IV A) the $^2P_{3/2}$ population starts growing immediately after the pulse. Transient measurements show that $^2P_{3/2}$ is populated maximally at $t=15\,\mu s$ (Fig. 5, right). Consequently, the luminescence spectra obtained with a delay of 15 μs after the laser pulse are largely dominated by emission originating from $^2P_{3/2}$. This is illustrated by Fig. 6, spectra (a2) and (b2): each consists of six peaks, corresponding to transitions from the lowest $^2P_{3/2}$ level to the six $^4I_{11/2}$ Stark levels of sites *A* and *B*, respectively. The luminescence spectra recorded without delay after the excitation pulse, on the other hand, also show transitions originating from $^4D_{3/2}$ in addition to the transitions originating from $^2P_{3/2}$. Thus the $^4D_{3/2} \rightarrow {}^4I_{13/2}$ and the $^2P_{3/2} \rightarrow {}^4I_{11/2}$ luminescence transitions are superimposed in Fig. 6, spectra (a1) and (b1). In addition to the six $^4I_{11/2}$ Stark levels, seven $^4I_{13/2}$ Stark levels are observed in each spectrum. The correctness of the Stark-level assignments for the two sites shown by the brackets in Fig. 6 is confirmed by site-selective $^4F_{3/2} \rightarrow {}^4I_{11/2}$ and $^4F_{3/2} \rightarrow {}^4I_{13/2}$ downconversion emission spectra (data not shown). The high-resolution upconversion luminescence spectra of Fig. 6 also illustrate the strict site-selectivity of the yellow to violet upconversion process: Emission from $^4D_{3/2}$ as well as $^2P_{3/2}$ emission exclusively occur from the originally excited site.

The $^4D_{3/2} \rightarrow {}^4I_{15/2}$ and $^2P_{3/2} \rightarrow {}^4I_{13/2}$ luminescence transitions around 22 000 cm^{-1} as well as the $^4D_{3/2} \rightarrow {}^4I_{11/2}$ and $^2P_{3/2} \rightarrow {}^4I_{9/2}$ transitions around 26 000 cm^{-1} can be deconvoluted in exactly the same way. Thus is it possible to determine the fractions of photons emitted from $^4D_{3/2}$ and $^2P_{3/2}$, respectively. In a $BaLu_2F_8$:0.6% Nd^{3+} crystal at 15 K this ratio is approximately 4:1 in both sites. In LaF_3:Nd^{3+} it is 15:1 and in $LiYF_4$:Nd^{3+} it is 0.6:1 at cryogenic temperatures.[20] Accordingly, the upconversion laser transitions in the latter two materials involve $^4D_{3/2}$ and $^2P_{3/2}$, respectively, as upper laser levels. In LaF_3:Nd^{3+} lasing was obtained on the $^4D_{3/2} \rightarrow {}^4I_{11/2}$ transition at 383 nm, in $LiYF_4$:Nd^{3+} the $^2P_{3/2} \rightarrow {}^4I_{11/2}$ transition lased at 414 nm.[12] As reported above, in $BaLu_2F_8$:0.6% Nd^{3+} luminescence from $^4D_{3/2}$ is four times stronger than from $^2P_{3/2}$. In addition, the strongest emission from $^4D_{3/2}$ is to the $^4I_{9/2}$ ground state.

There are two principal mechanisms by which upconversion can occur in our sample, namely the sequence of ground- and excited-state absorption steps (GSA/ESA) involving single ions and nonradiative energy-transfer upconversion (GSA/ETU) involving two excited ions.[21,22] Upconversion luminescence excitation spectra as well as the time evolution of the upconversion luminescence after an excitation pulse allow distinction between the above two processes. A GSA/ETU excitation spectrum is essentially the squared ground-state absorption spectrum of the excited state into which the upconversion excitation occurs, the reason being that the pathway by which the involved ions are excited to the intermediate state of the upconversion process is unimportant. Once this intermediate level is populated, the subsequent ETU step can be phonon-assisted and requires no exact energy resonance between the intermediate and the upper state involved in the upconversion process. The GSA/ESA mechanism, on the other hand, requires an exact energy resonance of the GSA and ESA steps. As a consequence the upconversion excitation spectrum resembles the product of the GSA and ESA spectra, and may therefore differ dramatically from the GSA spectrum of the excited state into which the excitation takes place, particularly in cases where both steps involve sharp transitions, such as the f-f transitions described here.

In our specific case we have to compare the $^4D_{3/2} \rightarrow {}^4I_{9/2}$ upconversion luminescence excitation spectra with the absorption spectrum of the $^4G_{5/2}+{}^2G_{7/2}$ multiplets in Fig. 7. Only the peaks of the site from which the upconversion luminescence is monitored appear in the excitation spectra. This is due to the site selectivity of the upconversion process. The $^4I_{9/2} \rightarrow {}^4G_{5/2}+{}^2G_{7/2}$ absorption spectrum, on the other hand, is a superposition of site-*A* and site-*B* absorption peaks, respectively. It is thus necessary to compare each of the two excitation spectra only with the peaks of the corresponding site in this absorption spectrum. This comparison shows that for both sites the upconversion excitation spectra clearly differ from their corresponding GSA spectra. This therefore indicates a dominant GSA/ESA upconversion mechanism.

Time-dependent measurements, i.e., probing the time evolution of the upconversion luminescence after an excitation pulse of a few nanoseconds width, provide a tool to distinguish unambiguously between the GSA/ETU and GSA/ESA upconversion mechanisms. In the latter case, both the GSA and the ESA step have to occur within the duration of the laser pulse. Consequently the upconversion luminescence decays instantaneously after the excitation pulse. In contrast, the typical GSA/ETU transient exhibits a rise in upconversion luminescence intensity followed by a decay. The rise and decay times are determined by both the intermediate and the upper excited-state lifetime. As shown in Fig. 5, after pulsed excitation into the $^4G_{5/2}$ and $^2G_{7/2}$ multiplets the resulting $^4D_{3/2} \rightarrow {}^4I_{9/2}$ upconversion luminescence intensity decays instantaneously after the laser pulse. The decay is single-exponential with the lifetime of the emitting $^4D_{3/2}$ excited state. We conclude that the yellow to violet upconversion mechanism is the one depicted in Fig. 10 (left). Excitation into the $^4G_{5/2}$ and $^2G_{7/2}$ multiplets leads to very rapid (<10 ns) multiphonon relaxation to the long-lived $^4F_{3/2}$ excited state, followed by $^4F_{3/2} \rightarrow {}^4D_{3/2,5/2,1/2}$ ESA. According to the upconversion excitation spectra of Fig. 7, efficient yellow to violet upconversion at 15 K is obtained for both sites after excitation at 17 259 cm^{-1}. From our $^4I_{9/2}$

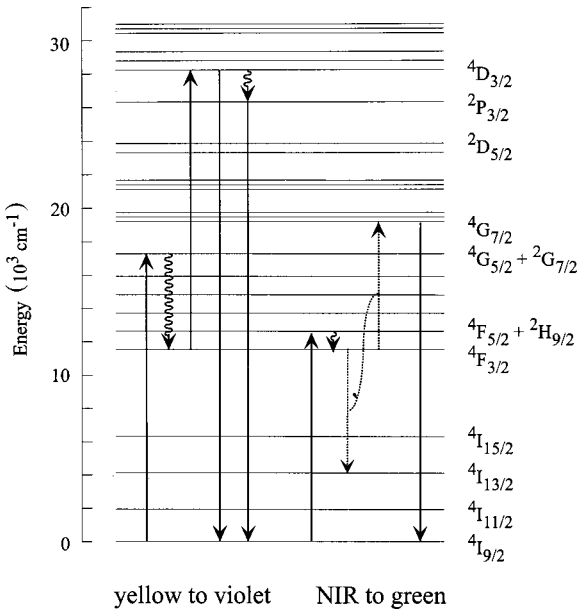

FIG. 10. Schematic representation of the upconversion mechanisms in $BaLu_2F_8$:0.6%Nd^{3+} after excitation of $^4G_{5/2}+{}^2G_{7/2}$ and $^4F_{5/2}+{}^2H_{9/2}$, respectively. Full arrows indicate radiative processes, wavy arrows indicate multiphonon relaxation events, and the connected dashed arrows indicate a nonradiative energy transfer process.

$\rightarrow {}^4G_{5/2}+{}^2G_{7/2}$ and $^4I_{9/2}\rightarrow {}^4D_{3/2,5/2,1/2}$ absorption spectra we would also expect GSA/ESA overlap peaks at energies between 17 100 and 17 200 cm^{-1}, which we do not observe in the upconversion excitation spectra (Fig. 7, middle, bottom). However, the exact energy-level positions of the two crystallographically distinct sites in the $^4D_{3/2,5/2,1/2}$ multiplets are not known. We explain the absence of the upconversion excitation peaks mentioned above by the strict site selectivity of the upconversion mechanism and a missing overlap of GSA and ESA of the *same site* at these energies.

C. Near-infrared to green upconversion

At cryogenic temperatures, excitation into the $^4F_{5/2}$ and $^2H_{9/2}$ multiplets around 12 500 cm^{-1} leads to $^4G_{7/2}\rightarrow {}^4I_{9/2}$ upconversion luminescence in the green spectral region (Fig. 8). This process is site-selective: unconverted green emission is only observed from the initially excited site. The weak site-*A* peaks in the site-*B* upconversion luminescence spectrum (Fig. 8, bottom) are due to a co-excitation of a small amount of site-*A* Nd^{3+} ions via a hot transition at 12 500 cm^{-1} as shown in the site-*A* upconversion excitation spectrum (Fig. 9, middle). Due to the small reduced energy gap of $p=3.4$ phonons between the emitting $^4G_{7/2}$ multiplet and its energetically next lower lying $^2G_{7/2}$ excited state, multiphonon relaxation is the dominant $^4G_{7/2}$-deactivation process. Thus radiative emission from the $^4G_{7/2}$ excited state is only weak and requires high excitation-power densities to be observed, especially when an upconversion process is involved. The $^4F_{5/2}$ multiplet is particularly favorable for near-infrared excitation of $^4G_{7/2}\rightarrow {}^4I_{9/2}$ upconversion luminescence due to its high molar extinction coefficients up to $25M^{-1}$ cm^{-1} as shown in the $^4I_{9/2}\rightarrow {}^4F_{5/2}+{}^2H_{9/2}$ absorption spectrum of Fig. 9, top.

In $LiYF_4$:1% Nd^{3+} the $^4G_{7/2}$ lifetime is 15 ns at 10 K.[23] In $BaLu_2F_8$:0.6% Nd^{3+}, after $^4F_{5/2}+{}^2H_{9/2}$ excitation with rectangular laser pulses we observe a decay of $^4G_{7/2}$ upconversion luminescence intensity that is three to four orders of magnitude slower: The best fits to these data yielded decay times of 99 and 102 μs for sites *A* and *B*, respectively. These long decay times, which are of the same order of magnitude as the $^4F_{3/2}$ lifetime, are due to nonradiative processes that feed $^4G_{7/2}$ after the exciting laser pulse. This fact and the absence of emission from the $^2G_{9/2}$ (around 21 000 cm^{-1}) and $^2P_{1/2}$ excited states (around 23 300 cm^{-1}), which have energy gaps to their energetically next lower lying multiplets similar to the gap below $^4G_{7/2}$, leads to the following mechanism: $^4F_{5/2}$ and $^2H_{9/2}$ excitation is followed by very fast (<10 ns) multiphonon relaxation to the $^4F_{3/2}$ intermediate state. From there a $^4F_{3/2}+{}^4F_{3/2}\rightarrow {}^4I_{13/2}+{}^4G_{7/2}$ ETU step occurs, i.e., one of two nearby excited Nd^{3+} ions transfers part of the excitation energy to its partner and relaxes itself to the $^4I_{13/2}$ excited state during this process (Fig. 10, right). This upconversion mechanism is in agreement with both the time-dependent results and the upconversion luminescence excitation spectra presented in Fig. 9 (middle, bottom). The sum of the latter two spectra is indeed very similar to the squared $^4I_{9/2}\rightarrow {}^4F_{5/2}+{}^2H_{9/2}$ absorption spectrum (Fig. 9, top). As stated in Sec. IV B this is one of the fingerprints of an ETU mechanism. The excitation spectra of Fig. 9 clearly show that at 15 K the ETU process is site-selective, i.e., energy transfer occurs only among Nd^{3+} ions doped into sites of the same type. This is due to a missing spectral overlap of $^4F_{3/2}\rightarrow {}^4I_{9/2}$ emission from one site with $^4I_{9/2}\rightarrow {}^4F_{3/2}$ absorption from the other site. On the other hand, for Nd^{3+} ions doped into sites of the same type this spectral overlap condition is very well fulfilled.

D. The role of the two crystallographically distinct sites: A comparison of $BaLu_2F_8$:0.6% Nd^{3+} and $BaLu_2F_8$:1.0% Er^{3+}

In 1% Er^{3+} doped $BaLu_2F_8$ an unidirectional intersite energy transfer was observed at 10 K in the $^4I_{11/2}$ excited state.[24] In $BaLu_2F_8$:0.6% Nd^{3+}, on the other hand, there is no communication between the two crystallographically different sites at temperatures below 30 K. The intersite energy transfer in the 1% Er^{3+} doped crystal occurs due to the spectral overlap of the $^4I_{11/2}\rightarrow {}^4I_{15/2}$ emission profile of the donor site *B* with the $^4I_{15/2}\rightarrow {}^4I_{11/2}$ GSA profile of the acceptor site *A*. At 10 K the energy-transfer rate constant of this process is $k_{ET}=830\,s^{-1}$, an order of magnitude faster than the decay rate constant of the $^4I_{11/2}$ excited state, which is $k_{rad}=80\,s^{-1}$. In $BaLu_2F_8$:0.6% Nd^{3+} the decay rate constant of the $^4F_{3/2}$ excited state is $k_{rad}=2500\,s^{-1}$, a factor of 3 larger than the intersite energy-transfer rate constant k_{ET} in $BaLu_2F_8$:1.0% Er^{3+}. In addition, at 15 K the spectral overlap of site *A* $^4F_{3/2}\rightarrow {}^4I_{9/2}$ emission with *B* $^4I_{9/2}\rightarrow {}^4F_{3/2}$ absorption is very small. As a result of both effects the $A\rightarrow B$ intersite energy-transfer rate is not competitive with the $^4F_{3/2}$ decay rate. Since the latter is the longest-lived excited state of the Nd^{3+} ion, intersite energy transfer is even less competitive in excited states other than $^4F_{3/2}$. Thus, 15-K upconversion is site-selective in $BaLu_2F_8$:0.6% Nd^{3+}, whereas in $BaLu_2F_8$:1% Er^{3+} upconversion luminescence

spectra are dominated by site-A emission due to the $B \rightarrow A$ intersite energy transfer in the $^4I_{11/2}$ intermediate state. This also reflects the fact that energy-transfer rates are generally larger in materials with higher dopant concentrations.

At temperatures above 30 K in $BaLu_2F_8$:0.6% Nd^{3+} intersite energy-transfer processes become important due to larger spectral overlaps of donor emission and acceptor absorption profiles caused by a broadening of the respective bands. As a consequence the site-selectivity of the upconversion is lost.

V. CONCLUSIONS

The new laser material $BaLu_2F_8$:Nd^{3+} was characterized spectroscopically via absorption, luminescence, excitation, and time-resolved experiments. Using excitation spectroscopic techniques the Stark levels of the most important multiplets involved in upconversion processes were assigned to the two crystallographically different Nd^{3+}-dopant sites. Yellow to violet upconversion occurs due to an overlap of the $^4I_{9/2} \rightarrow {}^4G_{5/2} + {}^2G_{7/2}$ GSA with the $^4F_{3/2} \rightarrow {}^4D_{3/2,5/2,1/2}$ ESA. For near-infrared to green upconversion a $^4F_{3/2} + {}^4F_{3/2} \rightarrow {}^4I_{13/2} + {}^4G_{7/2}$ ETU mechanism was found to be active.

Compared to more established materials such as $LiYF_4$:Nd^{3+}, LaF_3:Nd^{3+}, or BaY_2F_8:Nd^{3+} the density of states is increased by a factor of 2 in $BaLu_2F_8$:Nd^{3+} due to the presence of the two crystallographically distinct sites for the Nd^{3+} dopant ions. Due to this fact the spectral overlap between GSA and ESA is larger in this compound. This is only beneficial for upconversion efficiencies in the case of an intense communication between the Nd^{3+} ions doped into sites A and B. We have established the fact that in $BaLu_2F_8$:0.6% Nd^{3+} this is the case at room temperature, whereas at temperatures below 30 K the two sites act independently of each other.

Regarding a potential upconversion laser application it is noted that the $^4F_{3/2}$ lifetime of $BaLu_2F_8$:0.6% Nd^{3+} is essentially the same as that reported for the established upconversion laser material $LiYF_4$:Nd^{3+}.[14] The same is true for the room-temperature lifetimes of the blue- and violet-emitting $^2P_{3/2}$ and $^4D_{3/2}$ excited states. At cryogenic temperatures, on the other hand, the respective lifetimes are longer in $BaLu_2F_8$:0.6% Nd^{3+} by factors of 2 and 3, respectively. This facilitates the establishment of a population inversion between one of these excited states and a potential lower laser level. Unlike in $LiYF_4$:Nd^{3+} or LaF_3:Nd^{3+}, in $BaLu_2F_8$:0.6% Nd^{3+} the most intense upconversion luminescence is from the $^4D_{3/2}$ excited state to the $^4I_{9/2}$ ground state. This suggests the interesting possibility to use this high-energy transition ($\lambda = 356$ nm) as a laser transition. The large ground-state splitting of almost 500 cm^{-1} is favorable for this process. Based on this study we consider $BaLu_2F_8$:Nd^{3+} as a promising yellow to violet upconversion laser candidate and one deserving further study in that regard.

ACKNOWLEDGMENTS

Financial support by the Swiss National Science Foundation is gratefully acknowledged. The Russian authors wish to acknowledge partial financial support of the Russian Foundation for Basic Research and the State Scientific-Technical Program ''Fundamental Spectroscopy.''

[1] F. E. Auzel, C. R. Hebd. Seances Acad. Sci. **262**, 1016 (1960); **263**, 819 (1960).
[2] E. Downing, L. Hesselink, J. Ralston, and R. M. Macfarlane, Science **273**, 1185 (1987).
[3] W. Lenth and R. M. Macfarlane, Opt. Photonics News **3**, 8 (1992).
[4] R. Brede, T. Danger, E. Heumann, G. Huber, and B. H. T. Chai, Appl. Phys. Lett. **63**, 729 (1993).
[5] R. A. McFarlane, J. Opt. Soc. Am. B **11**, 871 (1994).
[6] G. K. Liu, Y. H. Chen, and J. V. Beitz, J. Lumin. **81**, 7 (1999).
[7] N. Pelletier-Allard and R. Pelletier, J. Lumin. **53**, 549 (1992).
[8] M. P. Hehlen, G. Frei, and Hans U. Güdel, Phys. Rev. B **50**, 16 264 (1994).
[9] A. A. Kaminskii, *Crystalline Lasers* (CRC, New York, 1996).
[10] A. A. Kaminskii, A. V. Butashin, J. Hulliger, Ph. Egger, S. N. Bagayev, H. J. Eicher, J. Findeisen, B. Liu, U. Täuber, P. Peuser, and S. N. Sulyanov, J. Alloys Compd. **275–277**, 442 (1998).
[11] I. Sirota, B. V. Bukvetskii, and V. I. Simonov, Krystallografiya **20**, 642 (1975) [Sov. Phys. Crystallogr. **20**, 393 (1975)].
[12] W. Lenth and R. M. Macfarlane, J. Lumin. **45**, 346 (1990).
[13] R. M. Macfarlane, F. Tong, A. J. Silversmith, and W. Lenth, Appl. Phys. Lett. **52**, 1300 (1988).
[14] T. Y. Fan, R. L. Byer, J. Opt. Soc. Am. B **3**, 1519 (1986).
[15] G. H. Dieke, *Spectra and Energy Levels of Rare Earth Ions in Crystals* (Wiley, New York, 1968).
[16] T. Riedener, K. Krämer, and H. U. Güdel, Inorg. Chem. **34**, 2745 (1995).
[17] J. M. F. van Dijk and H. W. Moos, Phys. Rev. **174**, 429 (1968).
[18] M. F. Joubert, B. Jacquier, R. M. Macfarlane, and C. Linares, J. Lumin. **47**, 269 (1991).
[19] M. Malinowski, B. Jacquier, M. Bouazaoui, M. F. Joubert, and C. Linares, Phys. Rev. B **41**, 31 (1990).
[20] B. Jacquier, M. Malinowski, M. F. Joubert, and R. M. Macfarlane, J. Lumin. **45**, 357 (1990).
[21] F. E. Auzel, Proc. IEEE **61**, 758 (1973).
[22] J. C. Wright, Top. Appl. Phys. **15**, 239 (1976).
[23] A. d. Novo-Gradac, W. M. Dennis, A. J. Silversmith, S. M. Jacobsen, and W. M. Yen, J. Lumin. **60&61**, 695 (1994).
[24] O. S. Wenger, D. R. Gamelin, A. V. Butashin, A. A. Kaminskii, and H. U. Güdel, Phys. Rev. B **60**, 5312 (1999).